Dynamic PCBM:Dimer Population in Solar Cells Under Light and Temperature Fluctuations

Sebastian Pont,[a,b] James R. Durrant,[a,b,c] * João T. Cabral[a,d] *

Photo-induced dimerization of phenyl-C61-butyric acid methyl ester (PCBM) has a significant impact on the stability of polymer:PCBM organic solar cells (OSC). This reaction is reversible, as dimers can be thermally decomposed at sufficiently elevated temperatures and both photo-dimerization and decomposition are temperature dependent. *In-operando* conditions of OSCs evidently involve exposure to both light and heat, following periodic diurnal and seasonal profiles. In this work, we examine and quantify the kinetics of dimer formation and decomposition as a function of temperature, light intensity, blend composition and time. We estimate the activation energy for photo-dimerization to be $0.021(3)\,\mathrm{eV}$, considerably smaller than that for decomposition ($0.96\,\mathrm{eV}$). We benchmark our findings with a variety of conjugated polymer matrices to propose a descriptive dynamic model of PCBM:dimer population in OSCs, and propose a framework to rationalize its interplay with morphology evolution and charge quenching. Our model and parameters enable the prediction of the dynamic and long-term PCBM:dimer populations, under variable temperature and light conditions, which impact the morphological stability of OSCs.

Keywords: dimerization, fullerenes, organic solar cells, photochemistry, stability

1 Introduction

Improvements in operational stability are required to realize the potential of organic solar cells (OSCs) with increasing power conversion efficiencies (PCE).[1] The current record certified efficiency is over 17 %[2] incorporating fullerene and non-fullerene electron acceptors in a tandem architecture. Novel polymers and device architectures are steadily increasing the performance of polymer:fullerene OSCs.[3–5] Evidently, the competitiveness of this technology is predicated on the achievement of long term stability, required for practical utilization. The loss of PCE over time can be attributed to numerous stress factors. Environmental elements such oxygen and humidity exposure can adversely affect performance, as well as mechanical failure, and robust encapsulation, mechanical and interfacial design are required to mitigate their effect. Intrinsic factors such as thermal stress, illumination, and interlayer-stability are, however, always present during operation.[6–8]

OSCs often experience a pronounced performance degradation during the initial stages of operation under illumination, which is termed 'burn-in', and attributed to several loss mechanisms currently under investigation.[9–11] One key mechanism has been related to be the photo-chemical dimerization of ubiquitous electron transporting material, phenyl-C61-butyric acid methyl ester (PCBM), and ensuing reduced charge mobility and the degradation in several polymer:fullerene systems.[12,13] However, other studies have found that photo-dimerization improves morphological stability and, in turn, device stability under thermal stress[14–16], while yet others have suggested neutral impact.[17] Recently, we reported a neutron reflectivity study on the competitive effects of light and temperature on the morphological stability of a polymer:fullerene blend.[18] These results found PCBM dimers to be effectively immobile compared to PCBM monomers in the blend matrix. The impact of PCBM dimerization on OSC performance appears thus non-trivial, and quantifying the PCBM dimer population throughout processing steps, at both short and long term operation conditions, is important to predict and improve OSC stability.

The photo-chemical dimerization (and polymerization) of C_{60} fullerenes was reported two decades ago by Eklund and coworkers,[19] who found cross-linking of up to 20 molecules upon photoirradiation of neat fullerene films. The reaction was found to be quenched by the presence of oxygen. Since oxygen is known to quench triplets in fullerenes to form singlet oxygen, dimerization was thus concluded to proceed via a triplet state. Using Raman spectroscopy, the reaction rate was found to be linear with irradiance (light intensity).[20] From these two observations it was suggested the fullerene 2+2 cycloaddition reaction proceeds via a triplet-ground state mechanism. The topo-chemical criteria require alignment of double bonds at less than 4.2 Å, with prescribed orientation (from 30×30=900 possible combinations for two fullerenes). Solid C_{60} exhibits an orientational ordering transition around 260 K, beyond which reaction rates increase considerably, due to increased likelihood of double bond alignment.[21] Upon further increasing temperature, thermal decomposition of polymeric C_{60} eventually occurs,[22] exhibiting an activation energy of 1.25 eV.

[a] *Centre for Plastic Electronics, Imperial College London, London, SW7 2AZ.*
[b] *Department of Chemistry, Imperial College London, London, SW7 2AZ.*
[c] *SPECIFIC IKC, College of Engineering, Swansea University, Bay Campus, SA1 8EN*
[d] *Department of Chemical Engineering, Imperial College London, London, SW7 2AZ*
* *Corresponding authors. Email: j.cabral@imperial.ac.uk, j.durrant@imperial.ac.uk*

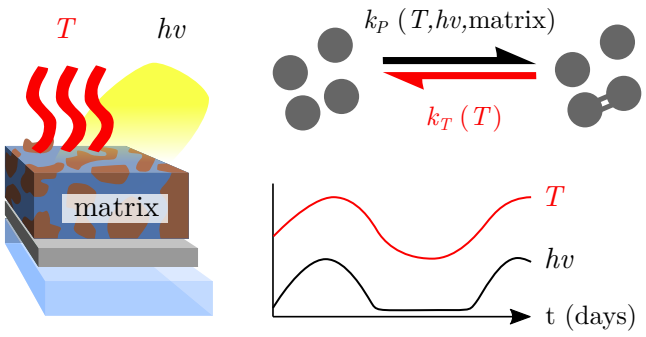

Figure 1 Schematic of $PC_{60}BM$ dimerization within the bulk heterojunction of a polymer:fullerene organic solar cell affected by temperature, light intensity, and the blend matrix. For each blend system and environment, a specific set of kinetic parameters determine the dynamic equilibrium of fullerene dimerization and decomposition. Our minimal model seeks to compute the monomer:dimer population balance over time.

The findings for C_{60} described above broadly apply to PCBM within polymer matrices, albeit with increased steric hindrance and perturbed topochemical, photophysical and dynamic conditions. Generally, photo-dimerization (instead of the formation of higher oligomers) prevails, as found by gel permeation chromatography (GPC) and Raman spectroscopy.[14,23] The thermally-induced de-dimerization in PCBM in PCDTBT was studied by Wong et al.[15], establishing that the kinetics were similar to those of C_{60}, albeit with an activation energy of 0.96 eV. Further, Edman and co-workers reported that the PCBM dimerization mechanism (in neat PCBM films) proceeds via a two triplet state.[24] A relatively complex dimerization assay involved the selective re-dissolution of the PCBM monomer in thin films following illumination. The height difference between illuminated and non-illuminated areas provided a quantification for the (insoluble) PCBM dimer fraction remaining. Using this method a non-linear relationship between dimerization and irradiance was proposed, suggesting a possible bi-excited reaction mechanism. Given that the excited singlet state lifetime is very short in PCBM, a triplet-triplet reaction was concluded to be most likely.[25] We note, however, the considerable variance in the data, potentially due to the complex assay of dimerization. More recent photophysics studies of the PCBM dimerization mechanism carried out by Brabec and co-workers[13] found that the quenching of PCBM photoluminescence by a photoactive polymer (PCPDTBT) correlated with the rate of dimerization. This suggests the mechanism proceeds via an excited state in the PCBM, corroborating earlier work on neat PCBM. By comparing four polymer:fullerene blends, the dimerization rate was found to correlate with the amorphous characteristics of the blend matrix. It was then suggested that better dispersion of PCBM molecules in amorphous systems might inhibit dimerization, as the likelihood of meeting the topochemical conditions decreases. Further, if the polymer matrix has the propensity for quenching triplet states, amorphous polymers are expected to do so more rapidly, which in turn also should affect the dimerization process.[26,27]

Alongside the photophysical mechanism of dimerization described above, it is important to consider the topological requirements of dimerization, namely the bond alignment and distance between neighboring fullerenes. In a polymer:fullerene blend system, there are a number of factors that will influence this including crystallinity,[28] domain size, component segregation (normal to the film surface)[29–31] and polymer:fullerene blend ratio[18]. Furthermore, time and temperature can non-trivially affect blend demixing and coarsening, crystallisation and surface segregation which, in turn, can modulate the local spatial arrangement of fullerenes and thus the statistics of meeting topochemical requirements.

Despite considerable experimental efforts, a precise understanding of the interplay between photo-chemistry, morphology and charge dynamics remains elusive. Whilst dimerization is known to be affected by light, temperature and the polymer matrix, a comprehensive model accounting for this wide parameter space has not been established. In this work, the rates and associated activation energy of photo-dimerization are computed from simultaneous illumination and annealing experiments. Further, we examine relationships between morphology and charge dynamics on dimerization. Alongside thermal decomposition kinetics, these results enable us to parameterize and construct a model for the evolution of PCBM:dimer populations, under prescribed illumination and thermal conditions and, specifically under diurnal and seasonal fluctuations associated with *in-operando* conditions. This challenge is in illustrated in Fig. 1. This minimal model allows dynamic predictions of dimerization of material systems subjected to a temporally varying environment, with implications for their operational stability.

2 Results and Discussion

2.1 Absorbance feature calibration

Upon illumination in an inert (N_2) atmosphere, PCBM dimerization results in a spectral UV-vis absorbance feature, that has been previously documented.[12,18] Figure 2(a) presents the absorbance of a PCDTBT:PCBM 1:2 thin film during 50 h illumination at 630 $W\,m^{-2}$ from a white LED (spectrum in Figure S1). Other methods used to quantify PCBM dimerization have several disadvantages: in Raman spectroscopy (visible, UV and even near IR), for instance, the illumination itself causes dimerization and thus is convoluted in the measurement outcome;[32] high performance liquid chromatography (HPLC) requires re-dissolution of the thin film (often with sonication) which can potentially cause both agglomeration and de-dimerization;[13] it is also comparatively time intensive. By contrast UV-vis absorbance assay used here is a facile approach, which is benchmarked in terms of absolute monomer:dimer concentration by calibration to ancillary gel permeation chromatography (GPC) measurements. This allows investigations of a much wider parameter space, range of systems and environmental factors.

Figure 2(b) presents GPC elution absorbance with peaks at 15.5 min, 18 min, and 19 min corresponding to PCDTBT, PCBM dimer, and PCBM monomer, respectively. By comparing the integrated intensity of the dimer and monomer peak, the absolute ra-

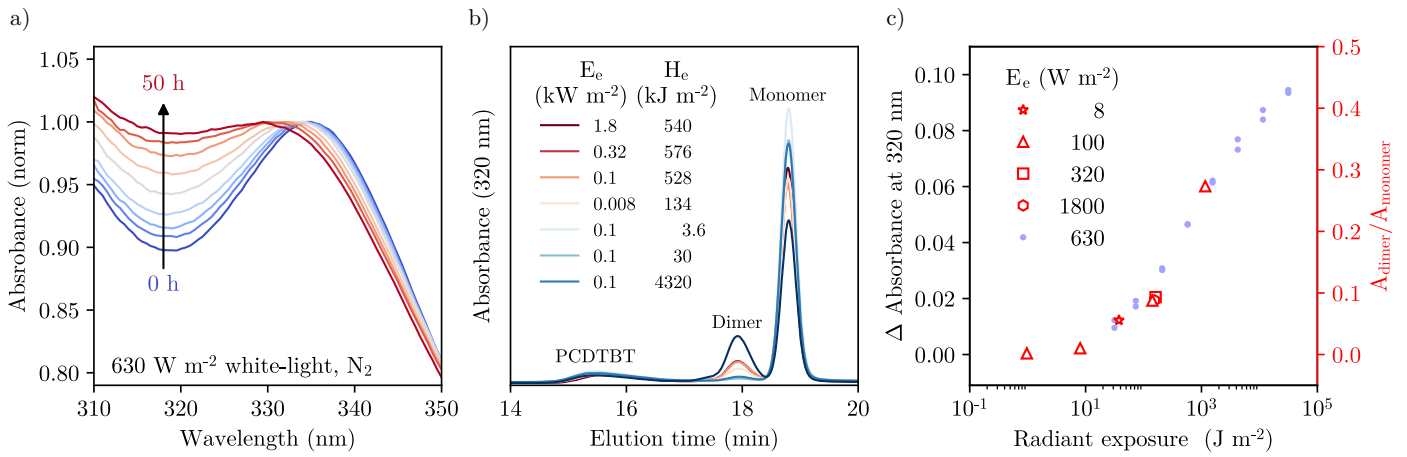

Figure 2 (a) Normalized absorbance spectra of PCDTBT:PCBM film over 50 h illumination at 630 W m^{-2} from a white LED in a nitrogen atmosphere. A feature change is observed at 320 nm due to the PCBM dimerization. (b) Gel permeation chromatography (GPC) of a PCDTBT:PCBM film after illumination at varying irradiance (E_e) and radiant exposure (H_e) from a white LED source. After illumination the monomer peak at 18.8 min decreases while the dimer peak at 17.9 min increases. (c) Correlated absorbance feature change at 320 nm, shown in (a), to the PCBM dimer:monomer ratio from the GPC measurement, shown in (b).

tio of dimer to monomer can be determined. To calibrate the absorbance assay to dimer concentration, a series of PCDTBT:PCBM films were illuminated at varying irradiance (E_e, or light intensity) and radiant exposures (H_e, or light dose). Figure 2(c) compares absorbance change at 320 nm to the dimer:monomer ratio from the GPC measurements for films soaked with varying radiant exposures. Over the small absorbance range, it is assumed the Beer-Lambert law can be simplified to a linear dependence on concentration. A clear correlation between the absorbance and the dimer ratio from GPC analysis is found, suggesting this assumption is valid. Illumination at constant radiant exposure with *varying* irradiance (red traces in Figure 2(b)) results in a constant dimer concentration. We thus conclude that dimerization is independent of irradiance, in line with previous findings.[20] From the direct correlation between GPC and absorbance measurements at 320 nm, we employ the latter as a quantitative (and facile) assay for dimerization.

2.2 Polymer:fullerene matrix dependence of k_P

The polymer:fullerene blend morphology, at the molecular and mesoscopic scales, is expected to control both the topo-chemical requirements and the photophysical mechanism of the dimerization reaction. To investigate the role of concentration on dimerization, we study model polystyrene (PS):PCBM blends with ratios of 1:4, 1:2, 1:1, 2:1, 4:1 supported on glass (although we find similar results when supported with PEDOT:PSS, as shown in Figure S2). Since films with lower PCBM loading have reduced absorbance, a spectral mismatch factor was applied to the radiant exposure. This factor was calculated by the integral between the white LED spectrum and the absorbance of the film (Figure S1). Over this series, blend morphology changes significantly from spinodal characteristics at 1:4 PS:PCBM loading (Figure 3(b) top), to clustering at 1:1 PS:PCBM (Figure 3(b) middle), and well-dispersed PCBM at 4:1 PS:PCBM ((Figure 3(b) bottom). AFM data for the entire series is presented in Figure S4(f). From the dimerization dependence on PCBM concentration, shown in Figure 3(a), it emerges that neither the rate nor conversion are significantly affected, with exception of the very low (4:1) PCBM loading, which is considerably lower than the remain. We hypothesize that, up to this concentration, sufficient PCBM is aggregated such that the topological requirements are not inhibited. Below this loading, PCBM is likely too dispersed and the reaction becomes limited by the distance between fullerenes. In summary, for this model system we find that concentration only affects dimerization at low PCBM concentrations that are rarely used in OSCs.

The photophysical properties of fullerene:polymer blends are expected to affect the rate of dimerization. PCBM triplet lifetimes are impacted by blend morphology: while in dispersed PCBM films, singlet exciton generation rapidly undergoes intersystem crossing to form triplets,[27] triplet yield is greatly inhibited in neat PCBM films. In PS:PCBM blends, the yield has been reported not to be significantly affected until very low loading of PCBM,[26] which is corroborated by the independence of PCBM dimerization with concentration presented in Figure 3(a). Alongside the photophysics, the amorphous or crystalline nature of the polymer matrix can be expected to impact the dimerization process, and dimerization has been reported to correlate favourably with increasing crystallinity.[13] The physical picture is that polymer crystallinity induces PCBM segregation and that, in turn, this increases the chance of meeting the topochemical requirements for dimerization. These results, for P3HT, KP115, SiPCPDTBT, PCPDTBT, in decreasing order of crystallinity, are compared alongside amorphous polymers PS and PCDTBT measured in this study in Figure 3(c), where all systems have a composition ratio of polymer:PCBM of 1:2. Morphological characterization (GIWAXS, NR, AFM) of the PCDTBT:PCBM and PS:PCBM samples are presented in Figure S4. Our first observation is that two amorphous polymer matrices (PS, PCDTBT) actually exhibit the largest dimer conversion of this polymer series; further, PCBM

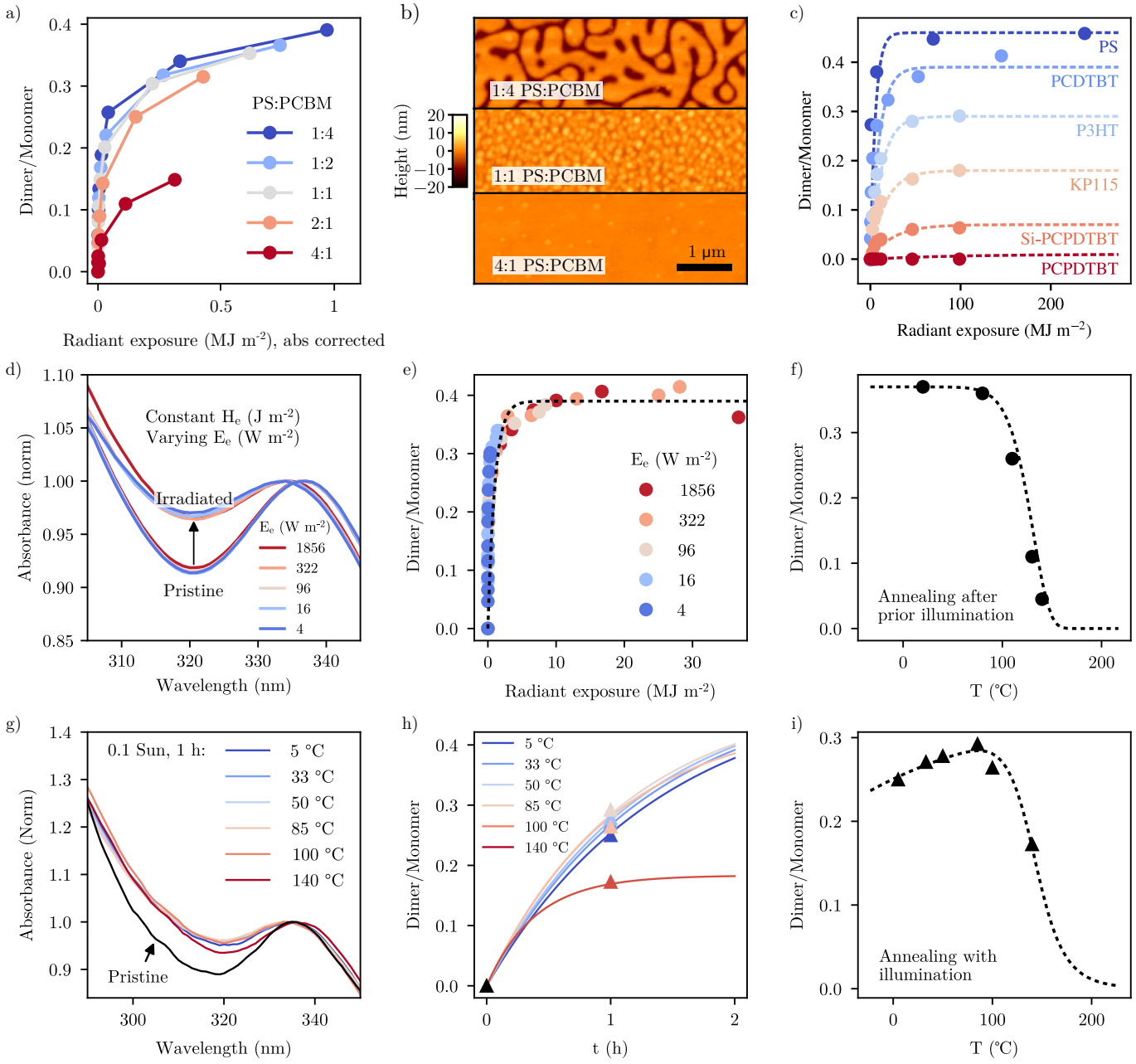

Figure 3 (a) PCBM dimer:monomer ratio of PS:PCBM at varying blend ratios with $96\,\mathrm{W\,m^{-2}}$ for $4\,\mathrm{h}$. The radiant exposure for has been corrected for absorbance variation relative to the 1:2 film. (b) Atomic force microscopy of three representative PS:PCBM blend films. A large variation in morphology between 1:4 (spinodal) and 1:1 (nucleation-like) yield similar rates of dimerization, while very asymmetric, PCBM-poor mixtures, with isolated cluster morphology at 4:1 ratio effectively hinder dimerization. (c) Dependence of the polymer matrix on dimerization for five polymer:PCBM (1:2) blends systems. Data for P3HT, KP115, Si-PCPDTBT, PCPDTBT was adapted from Ref[13]. (d) Absorbance of a PS:PCBM (1:2) film before and after $\approx 500\,\mathrm{J\,m^{-2}}$ radiant exposure (H_e) with irradiance (E_e) from $4\,\mathrm{W\,m^{-2}}$ to $1856\,\mathrm{W\,m^{-2}}$ (H_e, E_e, and t are detailed in Table S1). (e) Dimerization of a PS:PCBM (1:2) films with varying irradiance. Full absorbance spectra are given in Figure S3 and measurement details in Table S2. Irradiance independence corroborates a first-order triplet mechanism, suggested previously.[20,33] (f) PCDTBT:PCBM films with prior photo-dimerization to 0.36 dimer:monomer ($100\,\mathrm{W\,m^{-2}}$ for $4\,\mathrm{h}$) annealed in the dark for $1\,\mathrm{h}$, from our previous work.[15] The dashed line presents a fit to the dimerization reaction in Equation 1. (g) Normalized absorbance spectra of PS:PCBM films before (pristine) and after $1\,\mathrm{h}$ illumination at $100\,\mathrm{W\,m^{-2}}$ LED equivalent at temperatures from $5\,^{\circ}\mathrm{C}$ to $140\,^{\circ}\mathrm{C}$. (h) With the de-dimerization rate, k_T, known[15] the reaction model Equation 2 is fitted at temperature T and illumination $100\,\mathrm{W\,m^{-2}}$ to the data points of $D(t=0)$ and $D(t=1\ h)$ determined in (g). The solution gives temperature dependence of the dimerization rate, k_P. (i) The dimer concentration after $1\,\mathrm{h}$ illumination at $100\,\mathrm{W\,m^{-2}}$ for experimental results (triangles) and the solution of the reaction model (dashed line).

blends with PCPDTBT, another amorphous polymer (shown previously to effectively quench PCBM charges), exhibit negligible dimerization. Second, analysis of the fit parameters given in Supplementary Table S3 shows the rate of dimerization correlates with the saturation concentration, such that for PS:PCBM it shows the fast rate of photo-dimerization and also the greatest conversion. Evidently, the degree of crystallinity of the polymer matrix alone cannot be used as a predictor for the ability of PCBM to undergo photo-dimerization. In the case of PS, for instance, since it is not a photoactive polymer, the excited triplet state is not quenched, thus likely resulting in higher dimerization conversion. The interplay between blend morphology (including crystallinity) and specific blend photophysics must therefore be considered. We summarize our mechanistic understanding of the various factors affecting dimerization in the discussing section, after introducing a minimal framework to describe the dimer:monomer dynamics.

The dimer saturation concentration and pre-exponential factor reaction constant are both effected by the polymer matrix. From Figure 3(c) the steady-state concentration is found to vary from 0.46 in the PS:PCBM blend to below 0.08 for the Si-PCPDTBT:PCBM blend. The fraction of fullerenes available for dimerization is clearly dependent on the polymer matrix. For the blend systems compared in Figure 3(c), namely PS, PCDTBT, P3HT, KP115, and Si-PCPDTBT, the rate of dimerization is 0.18, 0.10, 0.08, 0.06, and $0.04\,\mathrm{MJ}^{-1}$ relative to the rate with PS (and negligible for PCPDTBT). The rate of dimerization is thus likely dependent on the quenching of the triplet states minimizing the chance of photo-dimerization and hence the reduced rate of dimerization.

2.3 Irradiance dependence of k_P

The intensity dependence of dimerization is a result of the photophysical mechanism. Reports on the dimerization of fullerenes have suggested both a mono-molecular (triplet)[20] and a bimolecular (triplet-triplet)[24] mechanism, as discussed in the introduction. To clarify this, PS:PCBM films were illuminated with irradiances over nearly three orders of magnitude, from $4\,\mathrm{W\,m^{-2}}$ to $1856\,\mathrm{W\,m^{-2}}$ (details of irradiance, radiant exposure, and time for each sample are given in Table S2). Analysis of the absorbance before and after approximately equal radiant exposure is presented in Figure 3(d). This result demonstrates that the absorbance feature change upon dimerization is independent of irradiance and therefore suggests that an equivalent process is occurring across all irradiances studied. The change in dimer concentration over time for five PS:PCBM films irradiated with varying irradiance is presented in Figure 3(e). This further demonstrations the dimerization is independent of irradiance. Therefore it is concluded PCBM dimerization proceeds via a monomolecular process involving a triplet state and a ground state. This result agrees with the work discussed in the introduction by Eklund and co-workers on C_{60}[20] but not with work by Edman and co-workers on PCBM.[24] The triplet driven cycloaddition reaction is well known in photochemistry. For example, within the DeMayo reaction mechanism or during the formation of mutagenic DNA in pyrimidine dimers which are the primary cause of melanomas in humans.[34,35] These reactions proceed via one triplet state that initiate the electrocyclic reactions.[36,37] It is thus likely that the fullerene photo-dimerization cycloaddition also follows a one triplet-state reaction mechanism we have observed.

2.4 Temperature dependence of k_P

The temperature dependence of the rates of reaction is required to simulate diurnal fluctuations of OSC *in-operando* conditions. The de-dimerization activation energy of both C_{60} and PCBM has previously been found with similar values at $1.25\,\mathrm{eV}$ and $0.96\,\mathrm{eV}$, respectively. The temperature dependence of the de-dimerization in PCDTBT:PCBM films is shown in Figure 3(f) with results previously reported by our group.[15] Films subjected to prior illumination were annealed at varying temperatures to monitor the rate of de-dimerization temperature dependence. The data fit well to a simple model (in the abasence of light) whereby the dimer concentration, D, at time t is given by $D(t) = D(t_0)\exp -(k_T t)$ and $\exp(k_T t)$.[22] Arrhenius analysis of the rate constant k_T versus temperature gives the relationship presented in Figure 4.

The temperature dependence of the photo-dimerization rate is also required to model systems under illumination and thermal stress. As the de-dimerization k_T is known, during simultaneous irradiance and annealing it is possible to determine the rate of dimerization, k_P. The photo-dimerization of PCBM was monitored after a constant radiant exposure at temperatures varying from $5\,^{\circ}\mathrm{C}$ to $140\,^{\circ}\mathrm{C}$. The absorbance spectrum was then measured and compared to a pristine sample, as shown in Figure 3(g). This was converted to dimer concentration using the calibration described earlier, and fitted with the previous reported[22] reaction material balance equation:

$$\frac{dD}{dt} = 0.5k_P \times I \times M(t) - k_T \times D(t) \tag{1}$$

where D is the dimer concentration, M is the monomer concentration, t is time, k_P is the rate of photo-dimerization, I is the light irradiance, k_T is the thermal de-dimerization. By substituting the molar balance $M(t) = M(t_0) - 2D(t)$ into Equation 1, it is possible to solve for the dimer concentration, D, at time t as describe in Equation 2, given the initial conditions of $D(t_0) = 0$.

$$D(t,I) = \frac{k_p \times I}{2(k_T + k_p \times I)}(1 - \exp(-(k_T + k_p \times I)t)) \tag{2}$$

With k_T known for all temperatures it is possible to solve Equation 2 to calculate k_P for each temperature in Figure 3(g). The solution to each equation is presented in Figure 3(h) and the dimer:monomer ratio after equal radiant exposure at different temperatures is presented in Figure 3(i). Qualitatively it is observed the rate of photo-induced dimerization decreases with temperature, hence the decrease from $100\,^{\circ}\mathrm{C}$ to $5\,^{\circ}\mathrm{C}$; while at temperatures above $120\,^{\circ}\mathrm{C}$ the thermally driven de-dimerization starts to dominate. By analyzing the Arrhenius temperature dependence of k_P, the activation energy of dimerization can be calculated to be $0.021(3)\,\mathrm{eV}$. This small temperature dependence is not unexpected for photochemical mechanism, and likely arises from the greater rotational freedom increasing the rate of bond alignment between fullerenes at higher temperatures.

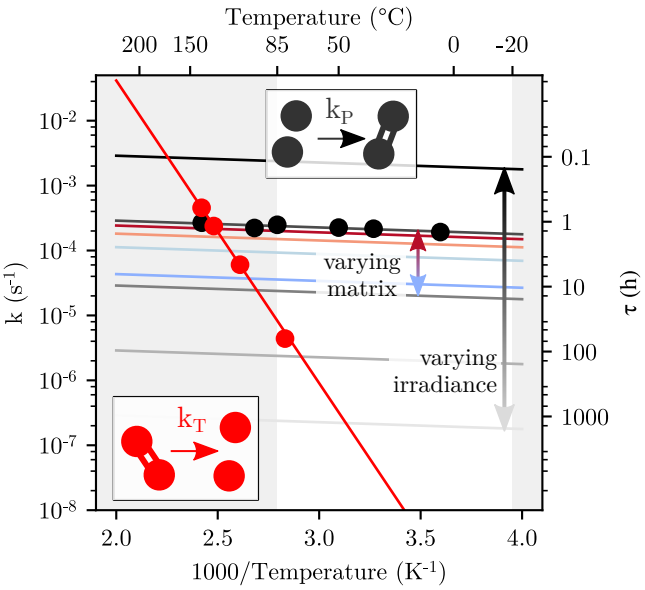

Figure 4 Thermal decomposition (or de-dimerization rate), k_T, dependence on temperature (experimental data shown by red circles, reproduced from Figure 3(f)) and the corresponding Arrhenius fit (red line). Photo-dimerization rate, k_P, at 0.1 Sun in a PS:PCBM film (experimental results (black circles, Figure 3(i)) and an Arrhenius fit (black line). The series of black lines present the effects of irradiances with the quickest rate at approximately 1 Sun equivalent, reducing in orders of magnitude. The series of red to blue lines present the effects of the polymer:fullerene matrix, adapted from Figure 3(c).

2.5 Arrhenius analysis

The interplay between dimer and monomer concentration at specific conditions of temperature and light intensity is dependent on the rate of the forward and backward reactions, each expressed as $k = A\exp(-E_a/k_BT)$ where A is the pre-exponential factor, E_a is the activation energy for the reaction, k_B is the Boltzmann constant, and T is the temperature. The rate constants calculated at various temperatures for k_T (Figure 3(f)) and k_P (Figure 3(i)) result in a good fit to the Arrhenius relationship, as presented in Figure 4. The photo-dimerization k_P has an activation energy of 0.021(3) eV and a pre-exponential factor of $4.69 \times 10^{-4}\,s^{-1}$ at $80.7\,W\,m^{-2}$. The de-dimerization has a much greater temperature dependence compared the photo-dimerization, as expected for a thermally-driven mechanism. The activation energy of the photo-dimerization is not expected to have a significant dependence on light intensity. In Figure 3(d,c) the rate is determined to be proportional to irradiance. Therefore the irradiance will result in a vertical translation of k_P in Figure 4. Light intensities were calculated for 1 Sun equivalent in a PS:PCBM film (topmost black line), decreasing in orders of magnitude. In the previous section, the polymer matrix was shown to affect the dimerization rate (Figure 3(c)), which is depicted in Figure 4 where the colors of red to blue correspond to the polymer:fullerene blends in Figure 3(c). Clearly, the reaction dynamics can occupy a large parameter space and the population equilibrium is strongly dependent on environmental conditions, even within the relatively narrow temperature range (indicated by the grey boundaries in Figure 4) relevant for the practical utilization of solar cells.

2.6 Modelling the long term stability of PCBM dimers

To simulate OSC *in-operando* conditions, the interplay of k_P and k_T with fluctuating light and temperature is considered. With the activation energy of dimerization and de-dimerization known it is possible to solve the differential reaction balance in Equation 1. The simulation can include diurnal variations of the conditions to calculate the changing rate constants (Figure 5(a,b)). To represent the *in-operando* temperature, a sinusoidal profile around the average temperature, $T_{average}$, is used. It has a period of 24 h and an amplitude of ±35 °C, as this is a typical diurnal fluctuation occurring within a solar module under operating conditions.[38] The light irradiance was modelled by a truncated sinusoidal with a period of 24 h, in phase with the temperature. Half the 24 h period has zero irradiance, corresponding to nighttime conditions. These models and subsequent rate constants are presented in Figure S5. The maximum and minimum population of PCBM monomer is based on analysis of PCDTBT but will be specific to the polymer:fullerene matrix, as shown in Figure 3(c). The effect of changing the average temperature is then investigated in terms of the dimer:monomer population by solving Equation 1 (Figure 5(c)). The solutions to three temperatures are highlighted in Figure 5: (I) Firstly, at lower temperatures the rate of dimerization is much greater than the rate of de-dimerization, such that the dimer dominates; (II) secondly, k_P and k_T are similar such that there are dynamic fluctuations during the diurnal light and temperature variations; (III) lastly, at higher temperatures the rate of de-dimerization dominates and the PCBM is mostly in the monomer form, but still continues to fluctuate during the 'day' period. At average temperatures below 50 °C photo-dimerization generally dominates, whereas for temperatures above 150 °C thermal de-dimerization dominates. Modelling of the PCDTBT:PCBM thin film suggests under operating conditions the PCBM dimer is likely to dominate over long time periods.

Within this model there are a number of variables that will affect the resulting dimer stability. These include the maximum daily irradiance, the diurnal temperature swing, and the initial PCBM dimer concentration. The maximum daily irradiance was varied from 0.01 to 10 Sun equivalent irradiance, as shown in Figure S6. At higher light irradiance there are considerably greater fluctuations in the diurnal period, whilst at lower irradiance it takes considerably longer to reach steady-state conditions. The effect of the initial PCBM dimer concentration (tuneable by light soaking during processing[14]) was also investigated (Figure S7) and found that, under the conditions modelled, the quasi-steady state is reached relatively quickly such that the initial concentration does not affect the system greatly. Finally, the diurnal temperature swing was varied from ±35 °C to ±0 °C, as shown in Figure S8. Two effects are observed when the average temperature swing is reduced from ±35 °C to ±0 °C: firstly, the diurnal population fluctuations increase and secondly that the average monomer concentration decreases. The examples presented here highlight the power of this simple model to implement a range of temperatures, irradiances, and polymer matrix conditions to simulate the PCBM dimer to monomer populations over time.

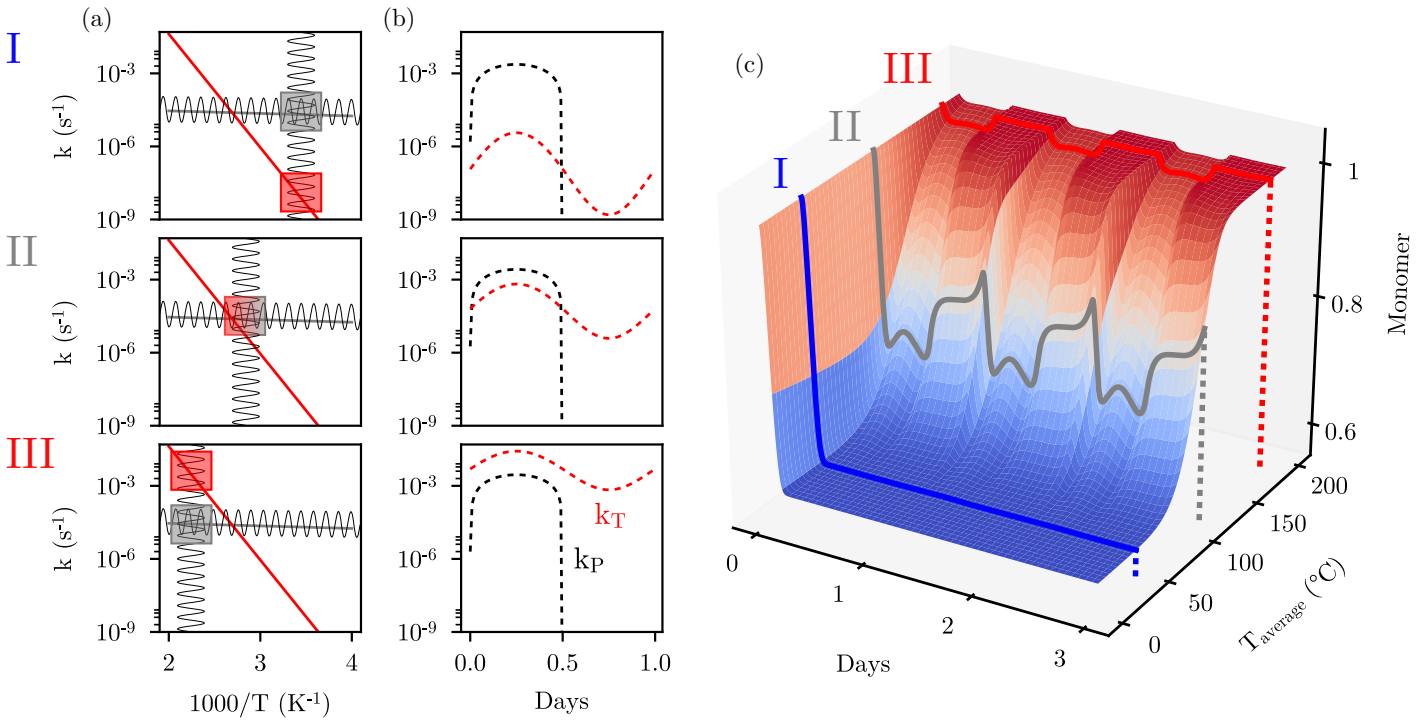

Figure 5 Representative simulated scenarios for dimerization with varying light and temperature obtained by solving Equation 1 with temporally varying environmental conditions (light and temperature exposure). The temperature profile is modelled as sinusoidal function with $T_{average} \pm 35\,^{\circ}\mathrm{C}$, while the illumination profile is modelled with a 12 h truncated sinusoidal function for the day and a 12 h zero rate for the night. These are shown in Figure S5. Three scenarios are illustrated for the relative magnitude of k_P and k_T (a,b) and the effect on the dimer population (c): (I) At $40\,^{\circ}\mathrm{C}$ the photo-dimerization dominates and the PCBM dimer concentration is saturated. (II) At $110\,^{\circ}\mathrm{C}$ $k_P \approx k_T$ resulting in large fluctuations in monomer:dimer ratio. (III) At $180\,^{\circ}\mathrm{C}$ $k_P \ll k_T$, de-dimerization dominates and PCBM remains predominately in monomer form.

2.7 Discussion

At the majority of relevant OSC operating conditions, our modelling results suggest that only moderate perturbations of PCBM dimer concentration will occur (Figure 4(c)). Given that the expected operating lifetime of solar panels is over 20 years, the numerous (10^3-10^4 diurnal cycles) light and temperature fluctuations are likely to impact OSC device performance.

The location of a OSC will have specific meteorological conditions of temperature and irradiance. The model results presented in Figure 5 assume a sinusoidal trend of environmental conditions. However, it is possible to input historical sensor readings of light and temperature of the point of application. This enables predictions of the long term dimer population in a specific location, and potentially the PCE stability.

Evidently, alongside the factors mentioned so far, blend morphology can also affect the dimerization process. Specifically, the local PCBM concentration will be modulated by the overall PCBM loading, as well as blend demixing, polymer crystallisation and surface segregation (to electrodes or film substrates). These will impact the ability of PCBM to meet topochemical requirements for photo-dimerization. Further, any spatio-temporal evolution of the active layer (e.g., as the operating temperature exceeds T_g of a given phase, enabling structural coarsening) will likely also affect the dimerization kinetics.[30] Such morphological changes over time are controlled by a range of factors and present theoretical and experimental challenges.[28,29] Moreover, blend photophysics can significantly affect charge quenching and thus the ability to photo-dimerize, and this process is, in turn, also affected by morphology. This complex coupling between local fullerene concentration, demixing and coarsening, crystallization, component segregation (normal to the film surface)—which are all potentially temperature and time-dependent—as well as the photophysics/charge quenching of the blend system is illustrated in Figure S9.

A first-principles predictive model of the dynamic PCBM:dimer population would thus need to explicitly consider all processes from the molecular to mesoscopic scales. Here, we have presented a facile method to (i) assay the rate of dimerization in a specific system and architecture and (ii) a minimal, descriptive, rate model to predict the subsequent dimerization within in-operando conditions of a solar cell. This two-step approach provides a powerful and facile means to predict the evolution of PCBM:dimer population in time and temperature and thus a practical strategy for the control of this important aspect of solar cell stability.

3 Conclusions

In summary, we present a minimal framework capable of describing the dynamic nature of PCBM fullerene photo-dimerization and decomposition, under varying environmental conditions of temperature and illumination. Model parameters are obtained by a systematic experimental study of the (coupled) effects of light exposure time and irradiance, as well as polymer matrix

and composition, and temperature. We comparatively examine experimental approaches to quantify dimerization and establish a facile UV-vis (320 nm) absorbance assay by ancillary GPC measurements. We establish the reaction rates and activation rates for both the forward and reverse reactions and obtain for the first time the activation energy of dimerization as $0.021(3)$ eV. Our results suggest that dimerization is *independent* of irradiance across three orders of magnitude encompassing the range relevant for practical applications, and that radiant exposure (the product of irradiance and time) is the relevant control variable. The nature of the polymer matrix, in terms of its impact in blend morphology and PCBM segregation, as well as photophysics, impacts primarily the prefactor of the dimerization reaction rate. We observe a significant decrease of the PCBM dimer population with temperature, in particular above $\approx$100 °C, where thermal decomposition becomes important. Under environmentally relevant operating conditions, however, we find that PCBM dimerization generally dominates. This means that a steady state asymptotic dimer population is rapidly attained, and is not significantly affected by temperature fluctuations (which could reverse it). This is caused by the near concurrence of exposure to high irradiance and elevated temperature and the fact that the forward reaction dominates in those circumstances, which we have now quantified. Our minimal model provides a predictive tool for PCBM dimerization in any polymer:fullerene blend matrix comprising the active layer of a solar cell, under any environmental condition (set by a time-varying temperature and light intensity profile), with a few and simple calibration steps. Such knowledge enables predictions for solar cell morphological stability and both short and long terms.

4 Experimental Section

Sample preparation. For the temperature dependent light soaking studies solutions of phenyl-C61-butyric acid methyl ester, PCBM, supplied by Nano-c, (Note only $PC_{60}BM$ was used in this study), PCDTBT supplied by 1-Material, and polystyrene, PS, with M_w =100 kg mol^{-1} (supplied by BDH Chemicals LTD) were prepared in chlorobenzene (25 mg mL^{-1}). Solutions were mixed in volumetric ratios to obtain required blend ratios. Glass substrates were plasma treated in an oxygen atmosphere with a Emitech K1050X before solutions were spin coated at 1500 rpm for 30 s. When used, PEDOT:PSS (Al 4083) was spun on glass substrates at 1000 rpm for 40 s before annealing at 100 °C for 20 min. The resulting film thicknesses of the polymer:PCBM was $\approx$100 nm, measured by stylus profilometry (Dektak XT). For the GPC measurements the samples were re-dissolved in chlorobenzene.

UV-visible absorption spectroscopy was carried out with a Shimadzu UV-1601 spectrophotometer with measurements taken from 300 nm to 350 nm in transmission mode and converted to absorbance. To determine an assay of PCBM dimer concentration the absorbance was normalized to a peak at $\approx$ 340 nm and the change at the peak minimum at $\approx$ 320 nm monitored.

Illumination and annealing was carried out in a nitrogen filled glovebox with oxygen and humidity levels kept < 15ppm. A Bridgelux 4000 K white LED light source was used with the spectrum shown in Figure S1. For thermal stress, temperatures were controlled with a hotplate or cooling plates and calibrated with an IR temperature sensor in the presence of the illumination to ensure accurate temperature control.

Gel permeation chromatography with in-situ optical measurements were performed using an Agilent Technologies 1260 Infinity GPC System with 1260 RID and DAD VL attachments. Measurements were performed at 80 °C, using analytical grade chlorobenzene as eluent with two PLgel 10 μm MIXED B columns in series. Samples were prepared using analytical grade chlorobenzene in concentrations of 1 mg mL^{-1} to 2 mg mL^{-1} and filtered with VWR PES membrane 0.45 μm syringe filters before submission. An injection volume of 50 μL and GPC flow rate of 1.00 mL min^{-1} was used. The absorbance at 300 nm, 320 nm, and 335 nm were used to monitor the elution and found to give equivalent results.

Atomic force microscopy (AFM) was carried out on a Bruker Innova microscope in tapping mode at 0.2 Hz with Si tips (MPP-11100-W, Bruker) to evaluate blend surface morphology.

GIWAXS Characterization was performed at beamline 5A at the Pohang Accelerator Laboratory (PAL) in South Korea. Samples were prepared on glass substrates. A 10 keV X-ray beam was employed at a grazing angle of 0.1°–0.16°, and scattering profiles recorded with a Dectris Pilatus 2M photon counting detector. In-plane data was taken at Q_Z = 0.01° and out-of-plane data at Q_{XY} = 0.0°.

Neutron reflectivity (NR) measurements were carried out at the D17 reflectometer at the Institut Laue Langevin (Grenoble, France). NR were employed to determine the cross-sectional structure of PCDTBT/PCBM and PS/PCBM films exposed to various environmental conditions. Measurements were performed at angles 0.9° and 3.4°, covering a momentum transfer normal to the surface ($Q_z = (4\pi/\lambda)\sin\theta$) ranging from 0.006 to 0.3 Å^{-1}. Specular reflectivity profiles were analyzed using Motofit[39].

Solving the reaction balance in Equation 1 was done using the scipy.integrate.odeint script in Python3.0 to integrate the differential equation.

5 Supporting Information

Supporting Information is available from the Wiley Online Library or from the author.

6 Acknowledgements

We thank the Engineering and Physical Sciences Research Council (EPSRC, UK, EP/L016702/1) and Solvay for financial support. Data presented in this paper are available on the Zenodo repository at 10.5281/zenodo.1313882. The authors would like to thank Jisu Hong and Chan Eon Park from Pohang University of Science and Technology (POSTECH) for assistance with GIWAXS measurements, Him Cheng Wong for selected AFM measurements, and the Institut Laue Langevin for beamtime.

References

1 S. A. Gevorgyan, M. V. Madsen, B. Roth, M. Corazza, M. Hösel, R. R. Søndergaard, M. Jørgensen and F. C. Krebs, *Advanced Energy Materials*, 2016, **6**, 1501208.

2 L. Meng, Y. Zhang, X. Wan, C. Li, X. Zhang, Y. Wang, X. Ke, Z. Xiao, L. Ding, R. Xia, H.-L. Yip, Y. Cao and Y. Chen, *Science*, 2018, **361**, 1094–1098.

3 J. Zhao, Y. Li, G. Yang, K. Jiang, H. Lin, H. Ade, W. Ma and H. Yan, *Nature Energy*, 2016, **1**, 15027.

4 S. Zhang, L. Ye and J. Hou, *Advanced Energy Materials*, 2016, **6**, 1–20.

5 W. Zhao, S. Li, H. Yao, S. Zhang, Y. Zhang, B. Yang and J. Hou, *Journal of the American Chemical Society*, 2017, **139**, 7148–7151.

6 H. K. H. Lee, A. M. Telford, J. A. Röhr, M. F. Wyatt, B. Rice, J. Wu, A. de Castro Maciel, S. M. Tuladhar, E. Speller, J. McGettrick, J. R. Searle, S. Pont, T. Watson, T. Kirchartz, J. R. Durrant, W. C. Tsoi, J. Nelson and Z. Li, *Energy & Environmental Science*, 2018, **11**, 417–428.

7 W. R. Mateker and M. D. McGehee, *Advanced Materials*, 2017, **29**, 1603940.

8 I. Fraga Domínguez, A. Distler and L. Lüer, *Advanced Energy Materials*, 2017, **7**, 1601320.

9 M. Jørgensen, K. Norrman, S. A. Gevorgyan, T. Tromholt, B. Andreasen and F. C. Krebs, *Advanced Materials*, 2012, **24**, 580–612.

10 S. Savagatrup, A. D. Printz, T. F. O'Connor, A. V. Zaretski, D. Rodriquez, E. J. Sawyer, K. M. Rajan, R. I. Acosta, S. E. Root and D. J. Lipomi, *Energy Environ. Sci.*, 2015, **8**, 55–80.

11 P. Cheng, C. Yan, Y. Wu, J. Wang, M. Qin, Q. An, J. Cao, L. Huo, F. Zhang, L. Ding, Y. Sun, W. Ma and X. Zhan, *Advanced Materials*, 2016, **28**, 8021–8028.

12 A. Distler, T. Sauermann, H.-J. Egelhaaf, S. Rodman, D. Waller, K.-S. Cheon, M. Lee and D. M. Guldi, *Advanced Energy Materials*, 2014, **4**, 1300693.

13 T. Heumueller, W. R. Mateker, A. Distler, U. F. Fritze, R. Cheacharoen, W. H. Nguyen, M. Biele, M. Salvador, M. von Delius, H.-J. Egelhaaf, M. D. McGehee and C. J. Brabec, *Energy Environ. Sci.*, 2016, **9**, 247–256.

14 Z. Li, H. C. Wong, Z. Huang, H. Zhong, C. H. Tan, W. C. Tsoi, J. S. Kim, J. R. Durrant and J. T. Cabral, *Nature communications*, 2013, **4**, 1–7.

15 H. C. Wong, Z. Li, C. H. Tan, H. Zhong, Z. Huang, H. Bronstein, I. McCulloch, J. T. Cabral and J. R. Durrant, *ACS Nano*, 2014, **8**, 1297–1308.

16 B. C. Schroeder, Z. Li, M. A. Brady, G. C. Faria, R. S. Ashraf, C. J. Takacs, J. S. Cowart, D. T. Duong, K. H. Chiu, C.-H. Tan, J. T. Cabral, A. Salleo, M. L. Chabinyc, J. R. Durrant and I. McCulloch, *Angewandte Chemie International Edition*, 2014, **53**, 12870–12875.

17 L. N. Inasaridze, A. I. Shames, I. V. Martynov, B. Li, A. V. Mumyatov, D. K. Susarova, E. A. Katz and P. A. Troshin, *J. Mater. Chem. A*, 2017, **5**, 8044–8050.

18 S. Pont, F. Foglia, A. M. Higgins, J. R. Durrant and J. T. Cabral, *Advanced Functional Materials*, 2018, **28**, 1802520.

19 A. Rao, K.-A. Wang, J. Holden, Y. Wang, P. Zhou, P. Eklund, C. Eloi and J. Robertson, *Journal of Materials Research*, 1993, **8**, 2277–2281.

20 Y. Wang, J. Holden, Z.-H. Dong, X.-X. Bi and P. Eklund, *Chemical Physics Letters*, 1993, **211**, 341–345.

21 P. Zhou, Z.-H. Dong, A. Rao and P. Eklund, *Chemical Physics Letters*, 1993, **211**, 337–340.

22 Y. Wang, J. Holden, X. X. Bi and P. Eklund, *Chemical Physics Letters*, 1994, **217**, 413–417.

23 F. Piersimoni, G. Degutis, S. Bertho, K. Vandewal, D. Spoltore, T. Vangerven, J. Drijkoningen, M. K. Van Bael, A. Hardy, J. D'Haen, W. Maes, D. Vanderzande, M. Nesladek and J. Manca, *Journal of Polymer Science Part B: Polymer Physics*, 2013, **51**, 1209–1214.

24 J. Wang, J. Enevold and L. Edman, *Advanced Functional Materials*, 2013, **23**, 3220–3225.

25 H. Wang, L. Whittaker-Brooks and G. R. Fleming, *J. Phys. Chem. C*, 2015, **34**, 19590âĂŞ19595.

26 S. Cook, H. Ohkita, Y. Kim, J. J. Benson-Smith, D. D. Bradley and J. R. Durrant, *Chemical Physics Letters*, 2007, **445**, 276–280.

27 C. Keiderling, S. Dimitrov and J. R. Durrant, *The Journal of Physical Chemistry C*, 2017, **121**, 14470–14475.

28 P. Müller-Buschbaum, *Advanced Materials*, 2014, **26**, 7692–7709.

29 K. Feron, S. Ulum, E. Sesa, B. B. Gong, W. J. Belcher, X. Zhou, C. J. Fell and P. C. Dastoor, *Journal of Applied Physics*, 2014, **116**, 124502.

30 C.-H. Tan, H. C. Wong, Z. Li, D. G. Bucknall, J. R. Durrant and J. T. Cabral, *Journal of Materials Chemistry C*, 2015, **3**, 9551–9558.

31 J. W. Kingsley, P. P. Marchisio, H. Yi, A. Iraqi, C. J. Kinane, S. Langridge, R. L. Thompson, A. J. Cadby, A. J. Pearson, D. G. Lidzey, R. A. L. Jones and A. J. Parnell, *Scientific Reports*, 2015, **4**, 5286.

32 P. van Loosdrecht, P. van Bentum and G. Meijer, *Chemical Physics Letters*, 1993, **205**, 191–196.

33 A. Distler, *PhD thesis*, University of Erlangen-Nuremberg, 2015.

34 D. S. Goodsell, *The Oncologist*, 2001, **6**, 298–299.

35 S. Poplata, A. Tröster, Y.-Q. Zou and T. Bach, *Chemical Reviews*, 2016, **116**, 9748–9815.

36 D. J. Hastings and A. C. Weedon, *Journal of the American Chemical Society*, 1991, **113**, 8525–8527.

37 S. Inagaki and K. Fukui, *Journal of the American Chemical Society*, 1975, **97**, 7480–7484.

38 S. G. Obukhov, I. A. Plotnikov, O. A. Surzhikova and K. D. Savkin, *IOP Conference Series: Materials Science and Engineering*, 2017, **189**, 012008.

39 A. Nelson, *Journal of Applied Crystallography*, 2006, **39**, 273–276.